

# Bound-state spectrum of an impurity in a quantum vortex

João E. H. Braz<sup>1</sup> and H. Terças<sup>2</sup>

<sup>1</sup>*CeFEMA, Instituto Superior Técnico, Universidade de Lisboa, Lisboa, Portugal*

<sup>2</sup>*IPFN, Instituto Superior Técnico, Universidade de Lisboa, Lisboa, Portugal*

We consider the problem of finding the bound-state spectrum of an impurity immersed in a weakly interacting two-dimensional Bose-Einstein condensate supporting a single vortex. We obtain approximate expressions for the energy levels and show that, due to the finite size of the condensate, the impurity can access only a finite number of physical bound states. By virtue of the topological quantization of the vorticity and of the emergence of the Tkachenko lattice, this system is promising as a robust and scalable platform for the realization of qubits. Moreover, it provides a potentially new paradigm for polaron physics in Bose-Einstein condensates and a glimpse towards the study of quantum turbulence in low-dimensionality systems.

## I. INTRODUCTION

The study of quantum many-body systems has a history of unveiling remarkable new physics upon the inclusion of *impurities* - particles distinct from those comprising the majority, due to their mass, spin, or charge. The understanding of such composite systems [1–4], along with the development of appropriate theoretical techniques, has been not only an enlightening process but also a necessary one, since the existence of impurities is inevitable in realizations of any physical system that condensed matter theory may aim to describe [5–7].

A paradigmatic example of the presence of impurities is the polaron, a quasi-particle resulting from the hybridization between an electron and a lattice phonon [8–10]. The weak electron-phonon coupling, the so-called Fröhlich polaron, initiated the understanding of phonon-mediated superconductivity [11–14], while recent progress in analytical and numerical techniques has allowed the description of more generic regimes [15–17].

Though firmly rooted in the phenomenology of solid-state physics, interest in analogue models of polaron physics by immersion of impurities in Bose-Einstein condensates (BEC) has grown in recent years [6, 18–23], a fact to be partially attributed to the high degree of controllability in ultracold-atom experiments. In one hand, impurities are ubiquitous in superfluid liquid Helium experiments and known to be at the origin of the pinning of vortex lines [1, 24]. This effect has been crucial for the experimental observation of vortices in superfluids by means of spectroscopic techniques, and therefore to the study of quantum turbulence [25–27]; in BECs, on the other hand, vortices can be produced in a controlled fashion [28–33], ranging from single-vortex realizations [31, 32] to the production of Tkachenko lattices [28, 33]. Most importantly, their stability is linked to a topological invariant quantizing the fluid angular momentum, making them as long-lived as the condensate itself [34]. In quasi-one dimensional BECs, the interaction of impurities with dark solitons has shown to be sufficiently rich to make possible a variety of applications in quantum information theory [35–37].

In this work, we investigate the eigenvalue problem of

an impurity bounded to a single vortex in a quasi two-dimensional (2D) condensate. In particular, we show that there is a tunable, finite number of bound states, making it a promising scheme for the realization of a qubit. This comes with advantages in respect to the one dimensional “dark-soliton qubit” considered in [35], as vortices are more stable in respect to the excitations of sound waves and offer additional flexibility regarding scalability, since the number of vortices that can be produced in a 2D dimensional rotating BEC (state-of-the-art Tkachenko lattices contain up to hundred vortices) is much larger than the few tens of solitons that one can produce in 1D traps.

This paper is organized as follows: In Sec. II, we set the basic equations describing the stationary vortex-impurity problem, where the vortex acts as a potential trapping the impurity. Upon establishing a variational approximation for the vortex profile, we solve the eigenvalue problem in Sec. III. In Sec. IV, we show how the finite size of the condensate determines which bound states are physical. In Sec. V, we discuss some experimental considerations towards the realization of this system. Finally, in Sec. VI, a discussion of the physical results and some concluding remarks are enclosed.

## II. STATIONARY SOLUTIONS OF THE WEAKLY INTERACTING VORTEX-IMPURITY SYSTEM

### A. The eigenvalue problem

We begin by considering the Gross-Pitaevskii equations (GPE) that describe the quasi two-dimensional (2D) BEC coupled to a single impurity, as

$$i\hbar\partial_t\psi_1 = -\frac{\hbar^2}{2m_1}\nabla^2\psi_1 + g_{11}|\psi_1|^2\psi_1 + g_{12}|\psi_2|^2\psi_1 \quad (1)$$

$$i\hbar\partial_t\psi_2 = -\frac{\hbar^2}{2m_2}\nabla^2\psi_2 + g_{12}|\psi_1|^2\psi_2. \quad (2)$$

Here,  $m_1$  and  $m_2$  respectively denote the BEC particle and the impurity masses,  $g_{11}$  is the interaction strength of the BEC particles and  $g_{12} = g_{21}$  stems from the

BEC-impurity interaction. For definiteness, we consider the case of repulsive interactions only,  $g_{11} > 0$  and  $g_{12} > 0$ . In the quasi two-dimensional situation,  $\xi = \hbar/\sqrt{2n_0m_1g_{11}}$  is the healing length, defining the typical size of the vortex core, where  $n_0 = N/A$  is the surface density of the condensate, with  $N$  being the total number of BEC particles and  $A$  the total area. Unless stated contrary, we perform the following calculations in the thermodynamic limit,  $N \rightarrow \infty$  and  $A \rightarrow \infty$ , while taking  $n_0$  constant. Within the present considerations, we obtain the stationary eigenvalue problem by extracting the time-dependence of Eqs. (2) as

$$\psi_1(\mathbf{r}, t) = \sqrt{n_0} \exp(-\frac{i}{\hbar}\mu t)\Phi(\mathbf{r}), \quad (3)$$

$$\psi_2(\mathbf{r}, t) = \frac{1}{\sqrt{\xi^2}} \exp(-\frac{i}{\hbar}Et)\Psi(\mathbf{r}), \quad (4)$$

where  $\mu$  is the BEC chemical potential and  $E$  some parameter of the impurity, to be defined later on. At zeroth order, i.e. by neglecting the effect of the impurity on the BEC dynamics, we defined the chemical potential as

$$\mu \simeq \frac{\hbar^2}{2m_1\xi^2} = n_0g_{11}. \quad (5)$$

As such, by performing the substitution  $\mathbf{r} \rightarrow \mathbf{r}/\xi$ , Eqs. (1) can be conveniently recast in a dimensionless form

$$\nabla^2\Phi + (1 - |\Phi|^2 - \kappa^2|\Psi|^2)\Phi = 0 \quad (6)$$

$$\nabla^2\Psi + (\epsilon - \gamma^2|\Phi|^2)\Psi = 0, \quad (7)$$

with  $\epsilon = 2m_2\xi^2E/\hbar^2$ , and the two parameters controlling the relative strength of the intra- and inter-particle interactions

$$\gamma^2 = \frac{g_{12}m_2}{g_{11}m_1}, \quad \kappa^2 = \frac{2m_1g_{12}}{\hbar^2}. \quad (8)$$

As we can see from Eqs. (6) and (7), there is a limit in which we can neglect the effect of the impurity on the BEC: making

$$\frac{\kappa^2}{\gamma^2} = \frac{m_1}{m_2} \frac{1}{n_0\xi^2} \rightarrow 0, \quad (9)$$

in the sense that  $\kappa^2$  vanishes as  $\gamma^2$  remains finite, Eq. (6) becomes decoupled from  $\Psi$ . In that limit, we may consider that the density  $|\Phi|^2$  acts as a potential of depth  $\gamma^2$  for  $\Psi$  in Eq. (7). In this weakly-interacting regime, we may handle the problem for the impurity as a linear one, in the sense that Eq. (7) amounts to the time-independent Schrödinger equation

$$H_{\text{imp}}\Psi = \epsilon\Psi, \quad (10)$$

with  $H_{\text{imp}}$  being the effective Hamiltonian,

$$H_{\text{imp}} = -\nabla^2 + \gamma^2|\Phi_0|^2, \quad (11)$$

where  $\Phi_0$  is the solution of Eq. (6) for  $\kappa^2 = 0$ .

## B. Vortex solution and the variational approximation

We are firstly interested in obtaining solutions to Eq. (6) in the limit  $\kappa \rightarrow 0$ ,

$$\nabla^2\Phi_0 + (1 - |\Phi_0|^2)\Phi_0 = 0, \quad (12)$$

which, in two dimensions, contains vortex solutions of the BEC [38, 39]. Here, we particularize to circularly symmetric solutions, i.e. configurations comprised of a single vortex at the origin. In polar coordinates, they read

$$\Phi_0(r, \varphi) = \phi(r)e^{in\varphi}, \quad \phi(r) \equiv |\Phi_0(r, 0)|, \quad (13)$$

with  $n$  being an integer, also known as the vortex charge. With this prescription, Eq (12) then becomes

$$\frac{d^2\phi}{dr^2} + \frac{1}{r}\frac{d\phi}{dr} - \frac{n^2}{r^2}\phi + (1 - \phi^2)\phi = 0. \quad (14)$$

The solution for  $n = 0$  is the trivial one (i.e. the homogeneous condensate), whereas solutions with  $|n| > 1$  are energetically unstable - multiply charged vortices decay in singly charged ones [40, 41]. In the following, we consider the case  $|n| = 1$ ; though this is the simplest non-trivial solution of (12), there are no known closed-form solutions of Eq. (14) [42]. Instead, we consider the asymptotic behaviour as  $r \rightarrow 0$  and  $r \rightarrow +\infty$  [42]

$$r \rightarrow 0: \quad \phi \propto r + \mathcal{O}(r^3), \quad (15)$$

$$r \rightarrow +\infty: \quad \phi = 1 - \frac{1}{2r^2} - \mathcal{O}(r^{-4}). \quad (16)$$

These asymptotics provides us with criteria to look for variational approximations to the solution of Eq. (14) [43]. In the present work, we consider a one-parameter family of trial functions of the form

$$\phi_\alpha(r) = \begin{cases} \frac{1}{2}\alpha r & , \quad 0 < r \leq r_\alpha \\ \sqrt{1 - \frac{1}{\alpha^2 r^2}} & , \quad r > r_\alpha \end{cases}, \quad (17)$$

where  $r_\alpha = \alpha^{-1}\sqrt{2}$  and  $\alpha$  is the variational parameter; this function is constructed to be continuous to first derivative for any  $\alpha \in \mathbb{R}^+$ . In turn, we find the value  $\alpha = \sqrt{5/6} \simeq 0.913$  to provide the optimal variational approximation within the family of functions of (17). A comparison with the numerical solution of Eq. (14) for  $|n| = 1$  is shown in Fig. 1.

## C. Impurity wave functions

We now substitute  $|\Phi_0|$  for  $\phi_\alpha$  in Eq. (10), in order to obtain *approximate* solutions for the impurity wave functions, and look for bound states, which amounts to

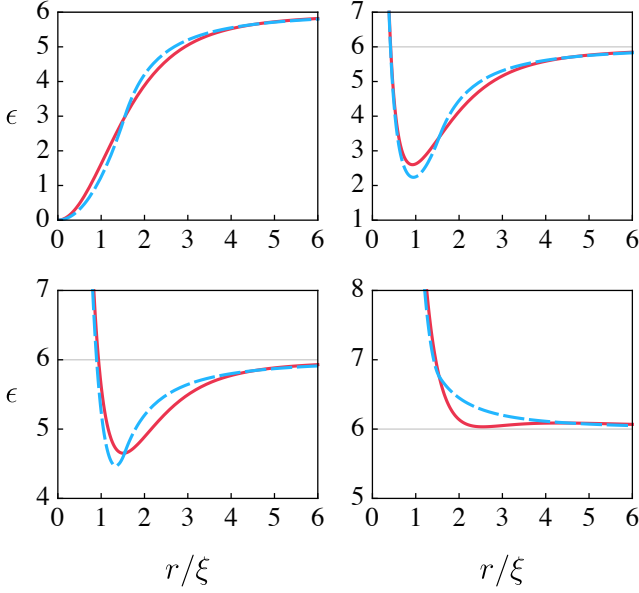


FIG. 1. (color online) Comparison of effective one-dimensional radial potentials for the exact solution (solid red) and the variational approximation of Eq. (17) (dashed blue), for  $\ell = 0$  (upper-left),  $\ell = 1$  (upper-right),  $\ell = 2$  (lower-left) and  $\ell = 3$  (lower-right), for a value  $\gamma^2 = 6$  (horizontal grey line) of the potential depth. We see that for  $\ell = 3$  the effective potentials are entirely above this line, illustrating the relation between the potential depth and angular momentum, and suggesting a loss of bound states for  $\gamma^2$  decreasing below some threshold.

requiring  $0 < \epsilon < \gamma^2$ . In polar coordinates, this is done by separating

$$\Psi(r, \varphi) = R(r)e^{\pm i\ell\varphi}, \quad (18)$$

with  $\ell = 0, 1, 2, \dots$  denoting the angular momentum. As for the radial part, it is solved in the two regions  $\mathcal{R}_1 = [0, r_\alpha]$  and  $\mathcal{R}_2 = (r_\alpha, \infty)$ . In the first region, we have

$$-\frac{d^2 R_1}{dr^2} - \frac{1}{r} \frac{dR_1}{dr} + \left( \frac{\ell^2}{r^2} + \frac{\alpha^2 \gamma^2}{4} r^2 \right) R_1 = \epsilon R_1. \quad (19)$$

Due to the term  $\ell^2/r^2$ , these solutions must scale as  $R_1(r) \propto r^\ell$  as  $r \rightarrow 0$  for each value of  $\ell$ , and so the correct solution is given by

$$R_1(r) = \mathcal{A} r^\ell e^{-\frac{\alpha\gamma}{4} r^2} \times M\left(-\frac{\epsilon}{2\alpha\gamma} + \frac{\ell+1}{2}, \ell+1; \frac{\alpha\gamma}{2} r^2\right), \quad (20)$$

where  $M(a, b; z)$  is the confluent hypergeometric function (CHF) with parameters  $a$  and  $b$ , also known as the first Kummer function [44], and  $\mathcal{A}$  is a normalization constant. Some relevant properties of this function are discussed in Appendix A. In turn, for the second region, we get

$$\frac{d^2 R_2}{dr^2} + \frac{1}{r} \frac{dR_2}{dr} + \frac{\gamma_\alpha^2 - \ell^2}{r^2} R_2 = (\gamma^2 - \epsilon) R_2, \quad (21)$$

where  $\gamma_\alpha = \gamma/\alpha$ . Here, the regular solution as required by the vanishing of the wave function as  $r \rightarrow +\infty$  is given by

$$R_2(r) = \mathcal{A} K_{i\lambda_\ell}(qr), \quad (22)$$

where  $\lambda_\ell = \sqrt{\gamma_\alpha^2 - \ell^2}$  and  $q = \sqrt{\gamma^2 - \epsilon}$  is a real number (for bound states), and  $K_{i\lambda_\ell}$  is the modified Bessel function of the second kind of *imaginary* order  $\lambda_\ell$  [44, 45]. Note that the character of the order (i.e. real or imaginary) does not affect the regularity of the solution (22) by itself [44], but it rather has a critical role in the bound-state spectrum of the impurity.

### III. BOUND-STATE SPECTRUM

The impurity spectrum in the vortex is obtained by requiring the continuity of the logarithmic derivative at  $r = r_\alpha$  [43],

$$(\ln R_1)'(r_\alpha) = (\ln R_2)'(r_\alpha), \quad (23)$$

and solving for  $q$ . Fig. 2 shows plots of these two functions. We find that Eq. (23) has no solutions for  $\gamma_\alpha \leq \ell$ , as shown in Appendix C 1, so we focus exclusively on the case  $\gamma_\alpha > \ell$ . Consequently, the condition  $\lambda_\ell = 0$  yields critical values  $\gamma_{c,\ell} = \alpha\ell$  for the onset of bound states of each angular momenta. Physically, we may interpret this behavior as the impurity seeing the vortex potential with an effective depth proportional to  $\lambda_\ell^2$ ; indeed, it is straightforward to check that, for each  $\ell$ , the effective radial potential has the maximum depth  $\alpha\gamma(\gamma_\alpha - \ell)$ . This suggests we can take  $\lambda_\ell$  (or, further, the related quantity  $\Delta_\ell \equiv \gamma_\alpha - \ell$ ), as the relevant scale of the problem. This point is illustrated in Fig. 1.

Since we are interested in a vortex with few bound states, as it is the case of a qubit, we focus on a parameter region

$$0 < \gamma_\alpha < 3. \quad (24)$$

Further, in order to obtain qualitative results from Eq. (23), we posit that in the present parameter range the states can be distinguished as shallow states and deep states: the former (latter) sit at the edge (bottom) of the potential, thus being characterized by the long-range, centripetal-like (short-range, harmonic oscillator-like) profile of the vortex density, as implied by Eq. (16) (Eq. (15)) and approximated, respectively, by each branch of Eq. (17).

#### A. Shallow states

In this case, we can expect  $q = \sqrt{\gamma^2 - \epsilon} \ll 1$ , prompting us to look for solutions of Eq. (23) to leading order in  $q$ . We thus use Eq. (B1) to obtain

$$(\ln R_2)'(r_\alpha) = \frac{\lambda_\ell}{r_\alpha} \cot\left(\lambda_\ell \ln \frac{qr_\alpha}{2} - \varphi_\ell\right) + \mathcal{O}(q^2), \quad (25)$$

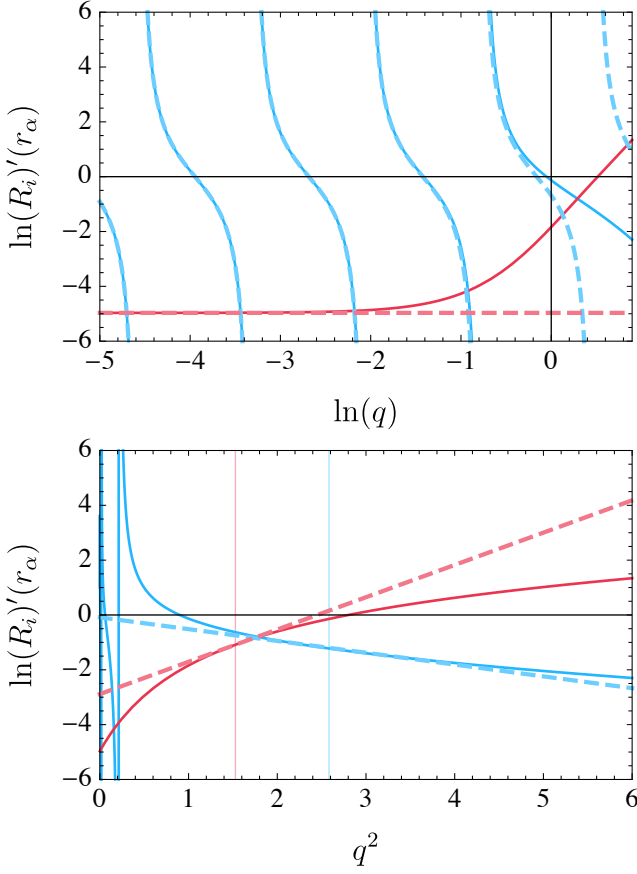


FIG. 2. (color online) An instance of Eq. (23) for  $\ell = 1$  and  $\gamma^2 = 6$ ; the function corresponding to region 1 (2), the deeper (shallower) end of the potential, is in thick red (blue); asymptotics and approximations are the dashed lines of respective color. (Upper panel) the choice of axis shows that there are infinitely many solutions (given by intersections) as  $q$  goes to zero, corresponding to shallow states, and the contribution from  $\mathcal{R}_1$  can be considered constant, while the contribution from  $\mathcal{R}_2$  is the RHS of (25); (lower panel) solutions for deep states can be obtained by linearization and asymptotics of the logarithmic derivatives, with the vertical lines indicating the linearization points.

where  $\varphi_\ell \equiv \varphi(\lambda_\ell)$  is related to the gamma function by  $\varphi(\lambda_\ell) = \arg \Gamma(1+i\lambda_\ell)$  [44, 45] (see B 1 for further details). For the LHS of Eq. (23), we have

$$(\ln R_1)'(r_\alpha) = -\frac{\lambda_\ell}{r_\alpha} \cot \theta_\ell + \mathcal{O}(q^2), \quad (26)$$

with

$$\theta_\ell = \tan^{-1} \left\{ \lambda_\ell \left[ \Delta_\ell - 2\gamma_\alpha \frac{M'(-\frac{\Delta_\ell}{2} + \frac{1}{2}, \ell+1; \gamma_\alpha)}{M(-\frac{\Delta_\ell}{2} + \frac{1}{2}, \ell+1; \gamma_\alpha)} \right]^{-1} \right\}, \quad (27)$$

where the prime represents differentiation with respect to the argument. The solution of Eq. (23), to leading order in  $q$ , finally yields the bound-state spectrum for shallow

states

$$\frac{E_{p,\ell}}{n_0 g_{12}} = 1 - \Lambda_\ell^2 \exp\left(-\frac{2\pi p}{\lambda_\ell}\right), \quad (28)$$

with  $p$  the radial quantum number, taking on non-negative integer values, and

$$\Lambda_\ell = \frac{\sqrt{2}}{\gamma_\alpha} \exp\left(-\frac{(1-\delta_{\ell,0})\pi + \theta_\ell - \varphi_\ell}{\lambda_\ell}\right), \quad (29)$$

where  $\delta_{\ell,0}$  is a Kronecker delta. The description of  $p$  must take into account the number of deep states: the integers  $p$  indicate the non-positive branches of the cotangent in (25) at which (23) has solutions, as illustrated in Fig. 2; as  $\gamma$  increases, Eq. (25) no longer holds for some values of  $p$ , as solutions transition from shallow to deep states; hence, the counting of  $p$  in (28) start from the number of deep states of angular momentum  $\ell$ , denoted here by  $N_d^{(\ell)}$  and discussed below.

## B. Deep states

Deep, or confined, states are considered according to the condition

$$\Delta_\ell > 1, \quad (30)$$

since, in this regime, it becomes possible for the first parameter of the CHF in Eq. (20) to take on non-positive values,

$$-\frac{\epsilon}{2\alpha\gamma} + \frac{\ell+1}{2} \leq 0, \quad (31)$$

from which (30) is obtained when  $\epsilon = \gamma^2$ , the highest possible value for bound states. If Eq. (31) is satisfied, the solutions to Eq. (20) become integrable on the whole plane, becoming the eigenfunctions of the isotropic quantum harmonic oscillator (check Appendix A 1 for a more complete discussion around this issue). This observation leads us to define the quantity

$$\delta\epsilon_1 \equiv -\frac{\epsilon}{2\alpha\gamma} + \frac{\ell+1}{2} + p, \quad (32)$$

for  $p = 0, 1, 2, \dots$ , and to look for solutions of Eq. (23) to first order in  $\delta\epsilon_1$  as the leading order contributions to its LHS. We thus require the first derivative of the CHF with respect to its first parameter evaluated at non-positive integers; one approach to this problem is presented in Appendix A 2.

Furthermore, the criterion in Eq. (30) can be easily generalized to a more precise condition regarding the number of deep states, and we find that

$$-1 < \Delta_\ell - 2N_d^{(\ell)} < 1, \quad (33)$$

for  $N_d^{(\ell)} = 0, 1, 2, \dots$ , if there are  $N_d^{(\ell)}$  deep states of angular momentum  $\pm\ell$ , accounting for the sign-degeneracy

in Eq. (18). Hence, within the parameter range given in (24), we have at most  $N_d^{(0)} = N_d^{(1)} = 1$  and  $N_d^{(2)} = 0$ , corresponding to the state  $p = 0$ , for  $\ell = 0$  and for  $\ell = 1$ , and none for  $\ell = 2$ . According to Eqs. (A4) and (A9), for  $p = 0$  the LHS of Eq. (23) becomes

$$(\ln R_1)'(r_\alpha) = -\frac{\Delta_\ell}{r_\alpha} + \frac{1}{r_\alpha} \frac{(\ell, \gamma_\alpha)!}{\gamma_\alpha^\ell e^{-\gamma_\alpha}} \left( \ell + 1 - \frac{\epsilon}{\alpha\gamma} \right) + \mathcal{O}(\delta\epsilon_1^2), \quad (34)$$

where  $(\ell, \gamma_\alpha)!$  is given in Eq. (A10). The RHS of Eq. (23), on the other hand, has a weak dependence on  $\epsilon$  for sufficiently large  $\gamma$ , since at that point the solution (22) transitions from an oscillatory to an exponentially decaying behavior, as discussed in B 2. We can write  $q = \lambda_\ell/r_\alpha + \delta\epsilon_2 + \mathcal{O}(\delta\epsilon_2^2)$ , and expand the RHS of Eq. (23) to first order in

$$\delta\epsilon_2 \equiv -\frac{\epsilon - (\gamma^2 - \lambda_\ell^2/r_\alpha^2)}{2\lambda_\ell/r_\alpha} = \frac{1}{r_\alpha} \left( \frac{\gamma_\alpha^2 + \ell^2}{2\lambda_\ell} - \frac{\epsilon}{\alpha^2\lambda_\ell} \right). \quad (35)$$

We then find

$$(\ln R_2)'(r_\alpha) = -\frac{\lambda_\ell \mathcal{K}_\ell}{r_\alpha} - \frac{\lambda_\ell \mathcal{K}_\ell^2}{r_\alpha} \left( \frac{\gamma_\alpha^2 + \ell^2}{2\lambda_\ell} - \frac{\epsilon}{\alpha^2\lambda_\ell} \right) + \mathcal{O}(\delta\epsilon_2^2), \quad (36)$$

where

$$\mathcal{K}_\ell \sim \frac{\beta}{\lambda_\ell^{1/3}} \left( 1 + \frac{1}{4\lambda_\ell} \right) + \mathcal{O}(\lambda_\ell^{-2}),$$

with  $\beta = 6^{1/3} \Gamma\left(\frac{2}{3}\right) / \Gamma\left(\frac{1}{3}\right) \approx 0.918$ , is an asymptotic approximation of  $\mathcal{K}_\ell \equiv -(\ln K_{i\lambda_\ell})'(\lambda_\ell)$  for large  $\lambda_\ell$ ; these results are derived in B 2. Equating (34) to (36) and solving in order to  $\delta\epsilon_1$ , yields

$$\frac{E_{p=0,\ell}}{\hbar\omega} = (\ell + 1)(1 - \Omega_\ell) + \left( \frac{\gamma_\alpha^2 + \ell^2}{2\gamma_\alpha} - \frac{\Delta_\ell - \lambda_\ell \mathcal{K}_\ell}{\gamma_\alpha \mathcal{K}_\ell^2} \right) \Omega_\ell \quad (37)$$

with

$$\Omega_\ell = \left( 1 + \frac{1}{\beta^2} \frac{\lambda_\ell^{5/3}}{\lambda_\ell + 1/2} \frac{(\ell, \gamma_\alpha)!}{\gamma_\alpha^{\ell+1} e^{-\gamma_\alpha}} \right)^{-1}, \quad (38)$$

and

$$\omega = \frac{\alpha}{2} \frac{\hbar}{m_2 \hat{\xi}^2}, \quad \hat{\xi}^2 = \frac{\hbar^2}{2n_0 \sqrt{g_{11} m_1 g_{12} m_2}}. \quad (39)$$

In particular, for  $\ell = 0$ , Eq. (37) gives the energy of the ground state, with (38) reducing to

$$\Omega_0 = \left( 1 + \frac{\gamma_\alpha^{2/3}}{\beta^2} \frac{e^{\gamma_\alpha} - 1}{\gamma_\alpha + 1/2} \right)^{-1}, \quad (40)$$

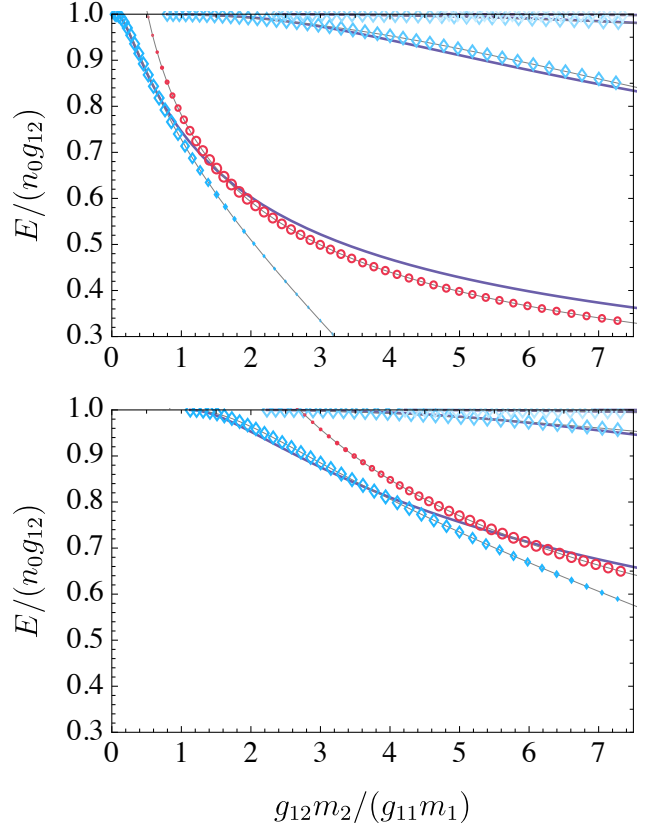


FIG. 3. (color online) Comparison of approximate to numerical results for  $\ell = 0$  (upper panel) and  $\ell = 1$  (lower panel). Each group of curves corresponds to a value of the radial quantum number  $p$ , starting from  $p = 0$ ; thick solid purple lines give the numerical solution; thin solid gray lines marked with blue diamonds (red circles) give the solutions from the shallow-state (deep-state) approximation, with the size of the markers being a function of the difference of approximate and numerical solutions for equal  $p$  at each  $\gamma^2$ . The finite-size cut-off corresponds to a trap of radius  $R = 1000$  healing lengths, according to Eq. (41), while the horizontal axis ranges within the interval (24).

for  $\gamma_\alpha > 1$ , i.e. whenever it is a deep state.

We can then write down the elements of the bound-state spectrum in the following way:

$$E_{p,\ell} = \begin{cases} n_0 g_{12} \mathcal{E}_{p,\ell}^{(s)} & , p - N_d^{(\ell)} \geq 0 \\ \hbar\omega \mathcal{E}_{p,\ell}^{(d)} & , p - N_d^{(\ell)} < 0 \end{cases},$$

where  $\mathcal{E}_{p,\ell}^{(s)}$  is given by the RHS of Eq. (28) and  $\mathcal{E}_{p=0,\ell}^{(d)}$  by the RHS of Eq. (37), and with  $N_d^{(\ell)}$  is determined for each  $\gamma^2$  according to (33) and the accuracy of the deep state approximation.

### C. Features of the energy spectrum

The energies of shallow and deep bound state are explicitly associated to two different energy scales  $n_0 g_{12}$



and  $\hbar\omega$ ; while the former is directly sourced from the microscopic dynamics of the system, being proportional to the interspecies coupling  $g_{12}$ , the latter can be written in terms of an emergent length scale that is *not* the characteristic healing length of the condensate, but rather a geometric mean

$$\hat{\xi} = \sqrt{\xi\zeta}, \quad \zeta^2 = \frac{\hbar^2}{2n_0m_2g_{12}},$$

where  $\zeta$  can be interpreted as an impurity-to-BEC penetration length. This interpretation becomes clearer by writing the square root of the dimensionless potential-well depth  $\gamma^2$  as

$$\gamma = \sqrt{\frac{g_{12}m_2}{g_{11}m_1}} = \frac{\xi}{\zeta},$$

and we see that an increase in depth of the potential can be interpreted, instead, as increased confinement according to the two emergent length scales. This also implies that, at least formally,  $\gamma^2$  may increase arbitrarily while  $\hat{\xi}$ , as well as  $\omega$ , remain finite. As depicted in Fig. 3, this disparity of scales indicates that, for each  $\ell$ , there can be a sizeable gap between deep states and shallow states relative to the gap between shallow states of different  $p$ .

Figure 3 shows excellent agreement between the approximate and numerical solutions, though there is a noticeable divergence with increasing  $\gamma$ . This is rooted in the variational approximation (17): notice that Eq. (37) tends to the spectrum of the harmonic oscillator with increasing  $\gamma$ , accordingly with the short-range behavior of the exact vortex profile (15). However, the slope at  $r = 0$  of the approximate solution (17) is smaller than that of the exact one, as fixed by the variational procedure. This discrepancy thus becomes starker with increased depth, with the spectrum of deep states being directly proportional to this slope as shown in Eq. (39).

An interesting feature of the impurity spectrum has to do with the energy levels near the edge of the potential. In this region, the spectrum is rich in crossovers and accidental degeneracies, resulting from the visibly faster decrease in energy of states of higher angular momenta. This can be understood in light of the competition between the centrifugal barrier and the vortex potential: at the onset of the first bound states, the long-range profile of the potential is canceled by the centrifugal term, rendering the effective potential more confining than that of states of lower angular momenta. This behavior is displayed in Fig. (4).

#### IV. FINITE SIZE AND PHYSICAL BOUND STATES

The spectrum obtained in Eq. (28) for the shallow states indicates that there are, in fact, infinitely many bound-state solutions for each  $\ell < \gamma_\alpha$ , which can be attributed to the slow algebraic growth of the vortex profile. Most of these are not physical solutions, however.

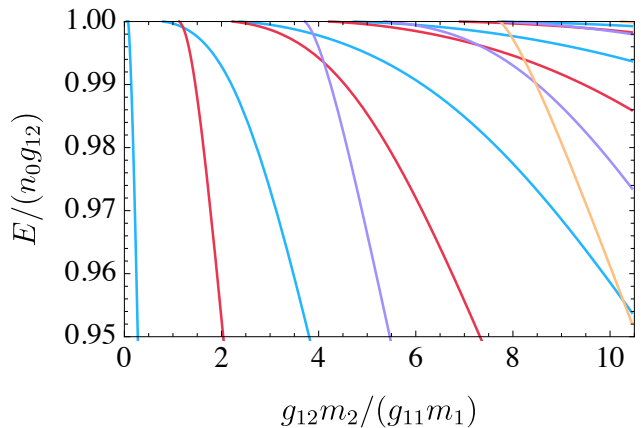


FIG. 4. (color online) Numerical values of the spectrum as a function of  $\gamma^2$  for  $\ell = 0$  (blue),  $\ell = 1$  (red),  $\ell = 2$  (purple) and  $\ell = 3$  (orange). Energy levels have a finite-size cut-off corresponding to a trap of radius  $R = 1000$  healing lengths.

To see this, we must consider that there is a natural cut-off imposed by the finite size of the trap, which is not merely a practical limitation: this is required by the stability of the vortex configuration, whose energy diverges logarithmically with the system size [46], and also due to the impossibility of long-range order in low dimensions, as imposed by the Mermin-Wagner theorem. We can account for this simply by requiring that the classical turning point (in the radial coordinate) of the putative bound state is lying within the domain of the BEC. Hence, assuming a disk-like trap of radius  $R \gg \xi$ , we have the quantitative condition

$$1 - \frac{E_{p,\ell}}{n_0 g_{12}} > \frac{\xi^2}{\alpha^2 R^2}, \quad (41)$$

which, together with Eq. (28), imposes a condition in  $\gamma^2$  for a bound state  $(p, \ell)$  to be contained in the BEC. Fig. (3) shows comparisons between numerical and approximate solutions, where the cut-off (41) for a trap of size  $R = 1000\xi$  was included. It is clear that for each value of  $\gamma$  there are only a finite number of bound states of the vortex, while those violating the condition Eq. (41) can be seen as bound states of the trapping potential.

Solutions to Eq. (41) can be found semi-analytically, as discussed in C2, yielding the critical condition

$$\left. \frac{g_{12}m_2}{g_{11}m_1} \right|_{p,\ell} > \alpha^2 \ell^2 + \frac{c_{p,\ell}^{-2}}{\ln\left(\frac{R}{r_{p,\ell}\xi}\right)^2} \quad (42)$$

for the onset of the bound state  $(p, \ell)$ . The coefficients  $c_{p,\ell}$  and  $r_{p,\ell}$  for the first few bound states are given in Table (I). Figure 5 gives a diagram of regimes of the vortex potential well, providing the number of bound states for each point in the  $(R/\xi, \gamma^2)$  parameter space.

Moreover, we can expect that imposing this cut-off *a posteriori* has negligible effects on the physical solutions of Eq. (10) since, in practice, the condition  $R \gg \xi$  is

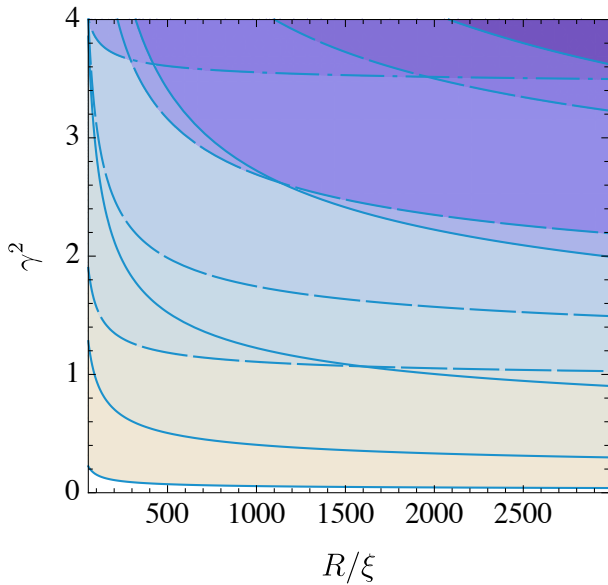


FIG. 5. (color online) Diagram of regimes of the vortex potential well, with the critical lines of (42) for  $\ell = 0$  (solid),  $\ell = 1$  (dashed) and  $\ell = 2$  (dot-dashed) bound states. For each point  $(R/\xi, \gamma^2)$  on the plane, the number of bound states is given by the number of curves below it, with a multiplicity of 2 for  $\ell \geq 1$  (e.g. the point (1000, 2.4) has  $3 + 2 \times 2 = 7$  bound states). Darker shades correspond to greater number of bound states.

implied by the thermodynamic limit. The caveat is that the possible highly-excited, highly-delocalized states may become affected by the trapping potential, but this correction can, in principle, be accounted for using perturbation theory. For this reason, the RHS of Eq. (42) is a tight lower bound of the critical value for the onset of the bound state  $(p, \ell)$ .

## V. EXPERIMENTAL CONSIDERATIONS

Recent experimental work with Yb- $^7\text{Li}$  mixtures [47] provides a realistic platform for the realization of this system: by virtue of the substantial mass imbalance of  $m_{\text{Yb}}/m_{\text{Li}} \approx 25$ , the impurity-to-vortex decoupling condition in Eq. (9) is within reach by immersion of Yb impurities (either fermionic  $^{173}\text{Yb}$ , or bosonic  $^{174}\text{Yb}$  [47]) in a  $^7\text{Li}$  condensate, while also increasing  $\gamma^2$ .

Nevertheless, the tunability of the latter is still necessary, since a vortex supporting only a few bound states requires  $\gamma^2$  one order of magnitude below that; thus, Feshbach resonances would be a crucial element in this realization. Coincidentally, the realizations of Ref. [47] exploits a fairly accessible Feshbach resonance of  $^7\text{Li}$  in order to produce a stable and sizeable BEC of this species [48]. The modest interspecies scattering found for Yb- $^7\text{Li}$  ( $\sim 1$  nm) [47] then means that the parameter range in Eq. (24) is well within reach by tuning the  $^7\text{Li}$  intra-species scattering to tens of nanometers.

In a quasi-2D BEC, such as considered presently, couplings become renormalized by the transversal length scale  $a_\perp$  of the harmonic trap [49–51], as  $g_{ij} \propto a_{ij}/a_\perp$  if  $a_{ij}$  is the scattering length between species  $i$  and  $j$ . While this multiplicative factor has no effect on  $\gamma^2 \propto g_{12}/g_{11}$ , the decoupling parameter  $\kappa^2/\gamma^2$  (see Eq. (9)) is proportional to  $g_{11}$  alone. Typical trapping frequencies of tens of kHz yield a transversal length of hundreds of nanometers for  $^7\text{Li}$ , which further reduces the decoupling parameter [52]. Additional flexibility comes from the usage of box potentials [53, 54], which are able to produce homogeneous condensates in a more controllable way [55, 56].

Another important aspect pertains to the relation of the energy scale  $n_0 g_{12}$  of the spectrum to the temperature. We find that for a peak density (in volume) of  $\sim 10^4 \text{ cm}^{-3}$ , the Yb- $^7\text{Li}$  mixture yields  $n_0 g_{12}/k_B \propto 10^2 \text{ nK}$ , meaning that the typical energy gap is much larger than the temperature of the system. This suggests that we might be in good position to further exploit these impurity bound states as physical qubits [35], thus paving the stage for a possible quantum information platform operating in the kHz range.

## VI. CONCLUSION

Starting from a variational ansatz for the vortex profile in a quasi two-dimensional Bose-Einstein condensate, which has been shown to be in excellent agreement with the numerical calculations, we have obtained the eigenstates and the eigenvalues of the vortex-impurity problem. Our method consists in imposing regularity conditions (continuity and finite derivative) at the crossing of the vortex piecewise solution, the point marking the transition between the core ( $\sim r$ , as  $r \rightarrow 0$ ) and the edge ( $\sim 1/r^2$ , as  $r \rightarrow \infty$ ) of the vortex. As a result, we are able to obtain analytic expression for both shallow and deep bound states, respectively lying at the edge and at the bottom of the effective potential experienced by the impurity when interacting with the vortex. A comparison with numerical results reveals that, for the states of angular momentum  $\ell = 0, 1$ , our analytical results appear to be accurate in their respective range of validity. For the general case, for states lying at the vortex profile transition, analytical expressions are, in general, not available explicitly. We point out that similar results have been obtained in the study of the one-dimensional  $1/x^2$  potential [57], and that a similar approach was used in the study of core-to-coreless vortex transition in multicomponent superfluids [58].

The consideration of heavy impurities immersed in a gas of light particles, as made possible by the recent experiments allowing for the controllable mixture of Li and Yb [47, 59, 60], allows the investigation of the polaron physics in a fashion opposed to the usual solid-state scenarios, where the impurity (electron) is much lighter than the host particles (ions) [8]. Moreover, our calculations may also contribute for future studies of the so-called

“Tkachenko polaron”, a quasi-particle resulting from the coupling between an impurity and a vortex lattice vibration in rotating Bose-Einstein condensates [61]. Here, the vortex-induced trapping may significantly change the features of the polaron.

More crucially, our findings show that it is possible to tune the value of the impurity-BEC interaction to isolate two deep (localized) bound states deep in the core of the vortex, making it possible to promote the impurity into a qubit, an essential element for applications in quantum information theory. In the future, it will be crucial to investigate the relevant beyond mean-field effects, namely the coupling with the quantum excitations of the BEC (phonons), a task that we believe essential for the complete characterization of the qubit performance. Due to the scalability of the number of vortices in a two-dimensional BEC, we expect this to become an interesting alternative to the one-dimensional qubits made of dark-solitons [37], therefore offering a possible alternative for a quantum information platform operating with acoustic degrees of freedom in a near future.

## ACKNOWLEDGMENTS

The authors acknowledge the financial support of FCT-Portugal through grant No. PD/BD/128625/2017 and through the contract number IF/00433/2015. JEHB would also like to thank the Joint Quantum Institute and the University of Maryland at College Park, for their hospitality during the writing of this manuscript, as well as the Fulbright Commission in Portugal. HT further acknowledges financial support from the Quantum Flagship Grant PhoQuS (820392) of the European Union.

## Appendix A: Properties of the confluent hypergeometric function

### 1. Zeros and monotonicity

The confluent hypergeometric function (CHF) can be expressed as a generalized hypergeometric series,

$$M(a, b; x) = \sum_{m=0}^{\infty} \frac{(a)_m}{(b)_m} \frac{x^m}{m!}, \quad (\text{A1})$$

where

$$(a)_m = \frac{\Gamma(a+m)}{\Gamma(a)} = a(a+1)\dots(a+m-1), \quad (\text{A2})$$

for any  $a \in \mathbb{C}$ , is the Pochhammer symbol, also known as the rising factorial; the CHF is an entire function of its argument, implying that the series (A1) has an infinite radius of convergence. [44]

From this definition, it is clear that for  $x \in [0, +\infty[$  the CHF has no zeros for any real  $a, b \geq 0$  and that it is positive and increasing. [44] Moreover, when  $a < 0$  it has  $\lceil -a \rceil$  positive zeros, and when  $a = -n$ , with  $n = 0, 1, 2, \dots$ , and  $b = \beta + 1$ , with  $\beta$  real and non-negative, the CHF reduces to the  $n$ th generalized Laguerre polynomial,

$$M(-n, \beta + 1; x) = \frac{n!}{(\beta + 1)_n} L_n^{(\beta)}(x); \quad (\text{A3})$$

the series in (A1) reduces to an  $n$ th-degree polynomial since  $(-n)_m$  vanishes for  $m \geq n - 1$ , as per (A2). [44] In particular, the generalized Laguerre polynomials comprise the solutions of the isotropic quantum harmonic oscillator. [44]

### 2. Derivative with respect to the first parameter

Suppose that in Eq. (A1) we have  $a = -n + \delta a$  with  $n = 0, 1, 2, \dots$ , with  $\delta a$  real and of small absolute value, and  $b = \beta + 1$ , with  $\beta$  real and non-negative. Taylor-expanding with regard to the first parameter we have

$$\begin{aligned} M(-n + \delta a, \beta + 1; x) &= \\ &= \frac{n!}{(\beta + 1)_n} L_n^{(\beta)}(x) + \delta a \tilde{M}_n^{(\beta)}(x) + O(\delta a^2), \end{aligned} \quad (\text{A4})$$

where we use (A3) for the zeroth-order term, and define

$$\tilde{M}_n^{(\beta)}(x) = \left. \frac{\partial}{\partial a} M(a, \beta + 1; x) \right|_{a=-n}, \quad (\text{A5})$$

for  $n = 0, 1, 2, \dots$ . For  $n = 0$ , we can use Eq. (38a) of Ref. [62] and rewrite it as

$$\tilde{M}_0^{(\beta)}(x) = \frac{1}{\beta + 1} \sum_{m=0}^{\infty} \frac{x^{m+1}}{(m+1)(\beta+2)_m}; \quad (\text{A6})$$

notice that

$$\frac{d}{dx} \tilde{M}_0^{(\beta)}(x) = \frac{1}{\beta + 1} M(1, \beta + 2; x),$$

since  $(1)_m = m!$  according to (A2); this CHF can be written as [44] (p. 328, Eq. (13.6.5))

$$M(1, \beta + 2; x) = (\beta + 1)x^{-\beta-1}e^x(\beta, x)!, \quad (\text{A7})$$

where  $(\beta, x)!$  is a rewriting of the incomplete gamma function [63],

$$(\beta, x)! = \gamma(\beta + 1, x) = \int_0^x dt t^\beta e^{-t}, \quad (\text{A8})$$

so that we can write (A6) as an integral of (A7):

$$\tilde{M}_0^{(\beta)}(x) = \int_0^x \frac{dy}{y} \frac{(\beta, y)!}{y^\beta e^{-y}}. \quad (\text{A9})$$



Further, for  $\beta = \ell$  a non-negative integer, it follows from (A8) that [44] (p. 177, Eq. (8.4.7))

$$\frac{(\ell, x)!}{\ell!} = 1 - e^{-x} \sum_{k=0}^{\ell} \frac{x^k}{k!}. \quad (\text{A10})$$

$$n = 1: \quad (\beta + 1) \tilde{M}_1^{(\beta)}(x) = -\frac{x}{\beta + 1} + \frac{(\beta, x)!}{x^\beta e^{-x}} + (1 + \beta - x) \int_0^x \frac{dy}{y} \frac{(\beta, y)!}{y^\beta e^{-y}}, \quad (\text{A12})$$

$$n \geq 2: \quad (\beta + n) \tilde{M}_n^{(\beta)}(x) - (2n + \beta - x - 1) \tilde{M}_{n-1}^{(\beta)}(x) + (n - 1) \tilde{M}_{n-2}^{(\beta)}(x) = \sum_{k=0}^2 \binom{2}{k} \frac{(-1)^k (n - k)!}{(\beta + 1)_{n-k}} L_{n-k}^{(\beta)}(x); \quad (\text{A13})$$

for  $n \geq 2$  we use (A3) to write the RHS in terms of generalized Laguerre polynomials, while for  $n = 1$  we use (A3), and (A7) along with the recurrence relation of the incomplete gamma function [44] (p. 178, Eq. (8.8.1))

$$\beta(\beta - 1, x)! = x^\beta e^{-x} + (\beta, x)!. \quad (\text{A14})$$

## Appendix B: Asymptotics of the Bessel- $K$ of imaginary order and its derivatives

### 1. Bessel- $K$ of imaginary order for small argument

For  $x \in \mathbb{R}^+$  small and  $\lambda \in \mathbb{R}^+$ , we have the limiting behavior [44, 45]

$$K_{i\lambda}(x) = -\sqrt{\frac{\pi}{\lambda \sinh(\pi\lambda)}} \sin\left(\lambda \ln \frac{x}{2} - \varphi(\lambda)\right) + \mathcal{O}(x^2), \quad (\text{B1})$$

where the function  $\varphi(\lambda)$  is given by

$$\varphi(\lambda) = \arg \Gamma(1 + i\lambda), \quad (\text{B2})$$

with the branch defined so that  $\varphi$  is continuous for  $0 < \lambda < \infty$  and  $\lim_{\lambda \rightarrow 0} \varphi(\lambda) = 0$  [45]. For large  $\lambda$ , this can be approximated using Stirling's formula [44], yielding

$$\varphi(\lambda) \sim \frac{\pi}{4} + \lambda (\ln \lambda - 1) + \mathcal{O}(\lambda^{-2}), \quad (\text{B3})$$

while for small  $\lambda$ , the gamma function can be approximated by the series [44] (p. 139, Eq. (5.7.3))

$$\begin{aligned} \log \Gamma(1 + z) &= -\log(1 + z) + (1 - \gamma_E)z \\ &+ \sum_{k=2}^{\infty} (-1)^k (\zeta(k) - 1) \frac{z^k}{k}, \end{aligned} \quad (\text{B4})$$

for  $|z| < 2$ , where  $\gamma_E \approx 0.5572$  is the Euler-Mascheroni constant and  $\zeta$  the Riemann-zeta function, giving

$$\varphi(\lambda) = -\gamma_E \lambda - \sum_{k=1}^{\infty} (-1)^k \frac{\zeta(2k+1)}{2k+1} \lambda^{2k+1}. \quad (\text{B5})$$

In turn, for  $n \geq 1$  we have [44] (p. 325, Eq. (13.3.1))

$$M(a, b; x) = \frac{(a - b)M(a - 1, b; x)}{2a - b + x} + \frac{aM(a + 1, b; x)}{2a - b + x}; \quad (\text{A11})$$

identifying parameters, expanding both sides to first order in  $\delta a$  and matching powers, we find

### 2. Bessel- $K$ of imaginary order at the transition point

In deriving Eq. (36), we perform a Taylor expansion

$$\begin{aligned} \left. \frac{d \ln K_{i\lambda_\ell}(qr)}{dr} \right|_{r=r_\alpha, q=\frac{\lambda_\ell}{r_\alpha} + \delta\epsilon_2} &= \\ &= -\frac{\lambda_\ell}{r_\alpha} \mathcal{K}_1(\lambda_\ell) - \delta\epsilon_2 (\mathcal{K}_1(\lambda_\ell) + \lambda_\ell \mathcal{K}_2(\lambda_\ell)) + \mathcal{O}(\delta\epsilon_2^2) \end{aligned} \quad (\text{B6})$$

where we define a family of functions specified as

$$\mathcal{K}_n(\lambda_\ell) = -(\ln K_{i\lambda_\ell})^{(n)}(\lambda_\ell), \quad (\text{B7})$$

that is, the  $n$ th derivative of the function  $-\ln K_{i\lambda_\ell}(x)$  evaluated at the so-called transition point  $x = \lambda_\ell$ . For  $n = 1, 2$ , we have explicitly

$$\mathcal{K}_1(\lambda_\ell) = -\frac{K'_{i\lambda_\ell}(\lambda_\ell)}{K_{i\lambda_\ell}(\lambda_\ell)}, \quad (\text{B8})$$

$$\mathcal{K}_2(\lambda_\ell) = -\frac{K''_{i\lambda_\ell}(\lambda_\ell)}{K_{i\lambda_\ell}(\lambda_\ell)} + \left(\frac{K'_{i\lambda_\ell}(\lambda_\ell)}{K_{i\lambda_\ell}(\lambda_\ell)}\right)^2, \quad (\text{B9})$$

where  $\lambda_\ell > \sqrt{2\ell + 1}$ ,  $\ell \in \mathbb{N}_0$ . Note that  $\mathcal{K}_\ell \equiv \mathcal{K}_1(\lambda_\ell)$ , as defined in the main text.

We have, for any  $z, \nu \in \mathbb{C}$  [44] (p. 252, Eqs. (10.29.2)),

$$K'_\nu(z) = \frac{\nu}{z} K_\nu(z) - K_{\nu+1}(z), \quad (\text{B10})$$

$$K''_\nu(z) = \left(1 + \frac{\nu(\nu - 1)}{z^2}\right) K_\nu(z) + \frac{1}{z} K_{\nu+1}(z); \quad (\text{B11})$$

in particular, for  $z = \lambda$  and  $\nu = i\lambda$ ,  $\lambda \in \mathbb{R}$ , we have

$$K'_{i\lambda}(\lambda) = iK_{i\lambda}(\lambda) - K_{1+i\lambda}(\lambda), \quad (\text{B12})$$

$$K_{i\lambda}''(\lambda) = -\frac{i}{\lambda}K_{i\lambda}(\lambda) + \frac{1}{\lambda}K_{1+i\lambda}(\lambda) = -\frac{1}{\lambda}K_{i\lambda}'(\lambda), \quad (\text{B13})$$

and then Eq. (B9) can then be written in terms of  $\mathcal{K}_\ell$  only as

$$\mathcal{K}_2(\lambda_\ell) = -\frac{\mathcal{K}_\ell}{\lambda_\ell} + \mathcal{K}_\ell^2. \quad (\text{B14})$$

Substituting (B14) into (B6), we obtain Eq. (36).

We have reduced the problem to computing asymptotic expressions of functions  $K_{i\lambda}(\lambda)$  and  $K_{i\lambda}'(\lambda)$  of  $\lambda$ , for  $\lambda > 1$ . We make use of the integral representation [44] (p. 252, Eq. (10.32.9))

$$K_\nu(z) = \int_0^\infty dt e^{-z \cosh t} \cosh(\nu t), \quad (\text{B15})$$

or  $|\text{ph}z| < \frac{\pi}{2}$  and any  $\nu \in \mathbb{C}$ . Substituting  $\nu = i\lambda$  and  $z = \lambda$ , we have

$$\begin{aligned} K_{i\lambda}(\lambda) &= \int_0^\infty dt e^{-\lambda \cosh t} \cos(\lambda t) \\ &= \frac{1}{2} \int_{-\infty}^{+\infty} dt e^{-\lambda \cosh t + i\lambda t}, \end{aligned} \quad (\text{B16})$$

and we find

$$K_{i\lambda}'(\lambda) = \frac{dK_{i\lambda}(\lambda)}{d\lambda} - \frac{1}{2} \int_{-\infty}^{+\infty} dt it e^{-\lambda \cosh t + i\lambda t}. \quad (\text{B17})$$

We can thus obtain asymptotic forms of  $K_{i\lambda}(\lambda)$  and  $K_{i\lambda}'(\lambda)$  from two  $\lambda$ -dependent integrals

$$\mathcal{I}_k = \frac{1}{2} \int_{-\infty}^{+\infty} dt (it)^k e^{-\lambda \cosh t + i\lambda t}, \quad k = 0, 1. \quad (\text{B18})$$

We note that  $\cosh t = 2 \sinh^2 \frac{t}{2} + 1$  and transform the integration coordinate as

$$\sinh \frac{t}{2} = \frac{x}{2} \Rightarrow dt = \frac{dx}{\sqrt{1 + \left(\frac{x}{2}\right)^2}},$$

yielding

$$\mathcal{I}_k = \frac{e^{-\lambda}}{2} \int_{-\infty}^{+\infty} dx \frac{e^{-\lambda g(x)}}{\sqrt{1 + \left(\frac{x}{2}\right)^2}} (it(x))^k, \quad k = 0, 1, \quad (\text{B19})$$

with  $t(x) = 2i \sinh^{-1} \frac{x}{2}$  and  $g(x) = \frac{x^2}{2} - 2i \sinh^{-1} \frac{x}{2}$ . We now perform a stationary phase approximation [64]: the function  $g$  is stationary for  $x = x_* = i\sqrt{2}$  and, expanding to subleading order in  $\xi = x - x_*$ , we have

$$g(x_* + \xi) = \left(\frac{\pi}{2} - 1\right) + \frac{i\sqrt{2}}{3}\xi^3 + \frac{\xi^4}{2} + \mathcal{O}(\xi^5). \quad (\text{B20})$$

Here, we include the subleading term to make a point that the integral is convergent; in what follows, however, we include only the leading order in  $\xi$  in the exponent, meaning we assume that contributions to the integral (B19) result dominantly from the oscillatory factor rather than from the decaying one, the latter granting only (implicitly) the convergence of the integral. We then have

$$\mathcal{I}_k \sim \frac{e^{-\frac{\pi\lambda}{2}}}{2} \int_{-\infty}^{+\infty} d\xi \frac{e^{-\frac{i\sqrt{2}\lambda}{3}\xi^3}}{\sqrt{1 + \left(\frac{x_* + \xi}{2}\right)^2}} p_k(\xi), \quad (\text{B21})$$

where we have made  $p_k(\xi) = (it(x_* + \xi))^k$ , so that  $p_0(\xi) = 1$  and

$$p_1(\xi) = -\frac{\pi}{2} + \sqrt{2}i\xi - \frac{1}{2}(i\xi)^2 + \frac{\sqrt{2}}{3}(i\xi)^3 - \frac{1}{2}(i\xi)^4 + \mathcal{O}(\xi^5). \quad (\text{B22})$$

Moreover, we consider that the variation of the denominator of the integrand is negligible in the presence of the exponential factor, so that we have

$$\int_{-\infty}^{+\infty} \frac{d\xi e^{-\frac{i\sqrt{2}\lambda}{3}\xi^3}}{\sqrt{1 + \left(\frac{x_* + \xi}{2}\right)^2}} p_k(\xi) \approx \sqrt{2} \int_{-\infty}^{+\infty} d\xi e^{-\frac{i\sqrt{2}\lambda}{3}\xi^3} p_k(\xi), \quad (\text{B23})$$

and, then,

$$\frac{1}{2} \int_{-\infty}^{+\infty} dx e^{-\frac{i\sqrt{2}\lambda}{3}\xi^3} p_k(\xi) = \text{Re} \left( \int_0^\infty d\xi e^{-\frac{i\sqrt{2}\lambda}{3}\xi^3} p_k(\xi) \right), \quad (\text{B24})$$

since  $p_k(-\xi)$  is the complex conjugate of  $p_k(\xi)$ . We have the integral identity in Ref. [65] (p. 337, Eq. (3.326.2.))

$$\int_0^\infty dx e^{-\beta x^n} x^m = \frac{\Gamma(\mu)}{n\beta^\mu}, \quad \mu = \frac{m+1}{n}, \quad (\text{B25})$$

for  $\text{Re}\beta, \text{Re}m, \text{Re}n > 0$  [66]. Thus, for the integral of (B24), we will have

$$\begin{aligned} &\text{Re} \left( \sqrt{2} \int_0^\infty d\xi e^{-\frac{i\sqrt{2}\lambda}{3}\xi^3} (i\xi)^m \right) \\ &= \frac{1}{3} \cos \left( \frac{\pi}{2} \frac{2m-1}{3} \right) \frac{6^{\frac{m+1}{3}} \Gamma\left(\frac{m+1}{3}\right)}{2^{\frac{m}{2}} \lambda^{\frac{m+1}{3}}}, \end{aligned} \quad (\text{B26})$$

and we arrive at

$$K_{i\lambda}(\lambda) = \mathcal{I}_0 \sim \frac{e^{-\frac{\pi\lambda}{2}}}{2\sqrt{3}} \frac{6^{\frac{1}{3}} \Gamma\left(\frac{1}{3}\right)}{\lambda^{\frac{1}{3}}}, \quad (\text{B27})$$

$$K_{i\lambda}'(\lambda) = \frac{d\mathcal{I}_0}{d\lambda} - \mathcal{I}_1 \sim -\frac{e^{-\frac{\pi\lambda}{2}}}{2\sqrt{3}} \frac{6^{\frac{2}{3}} \Gamma\left(\frac{2}{3}\right)}{\lambda^{\frac{2}{3}}} \left(1 + \frac{1}{4\lambda}\right) + \mathcal{O}(\lambda^{-2}), \quad (\text{B28})$$

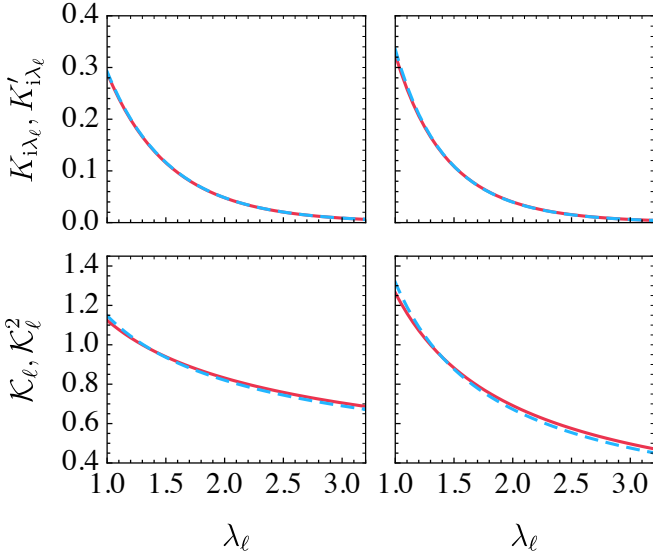


FIG. 6. Comparison of asymptotic approximations (dashed blue) and exact functions (solid red); top-right  $K_{i\lambda_\ell}$ , top-left  $K'_{i\lambda_\ell}$ , bottom-right  $\mathcal{K}_\ell$  and bottom-left  $\mathcal{K}_\ell^2$ . The horizontal axis ranges within the interval (24) for  $\lambda_\ell > 1$ , for each  $\ell$ .

and, moreover,

$$\mathcal{K}_\ell = -\frac{K'_{i\lambda_\ell}(\lambda_\ell)}{K_{i\lambda_\ell}(\lambda_\ell)} \sim \frac{\kappa}{\lambda_\ell^{1/3}} \left(1 + \frac{1}{4\lambda_\ell}\right) + \mathcal{O}(\lambda_\ell^{-2}), \quad (\text{B29})$$

with  $\kappa = 6^{1/3} \Gamma\left(\frac{2}{3}\right) / \Gamma\left(\frac{1}{3}\right) \approx 0.918$ . Fig. 6 shows a comparison of the exact functions and respective asymptotic approximations. Moreover, these appear to be in agreement with the formulas provided in Ref. [67] (p. 142, 2nd eq.).

### Appendix C: Onset of bound states

#### 1. Nonexistence of bound states of angular momenta $\ell \geq \gamma_\alpha$

We show that whenever  $\Delta_\ell = \gamma_\alpha - \ell \leq 0$ , Eq. (23) has no solutions for  $q$  real and positive.

We note that  $K_\nu(x)$  of real order  $\nu$  is a positive and decreasing function of  $x \in ]0, +\infty[$ , hence we have

$$(\ln R_2)'(r_\alpha) = q \frac{K'_\nu(qr_\alpha)}{K_\nu(qr_\alpha)} < 0 \quad (\text{C1})$$

for all  $q > 0$ , where  $\nu = \sqrt{\ell^2 - \gamma_\alpha^2}$ . It follows that solutions of (23) would require

$$(\ln R_1)'(r_\alpha) < 0. \quad (\text{C2})$$

In turn, according to the properties of the CHF for positive parameters presented in Appendix A 1, it follows

that

$$\begin{aligned} (\ln R_1)'(r_\alpha) &= \\ &= \frac{|\Delta_\ell|}{r_\alpha} + \frac{2\gamma_\alpha}{r_\alpha} \frac{M'\left(\frac{1}{2}|\Delta_\ell| + \frac{q^2}{2\alpha\gamma} + \frac{1}{2}, \ell + 1; \gamma_\alpha\right)}{M\left(\frac{1}{2}|\Delta_\ell| + \frac{q^2}{2\alpha\gamma} + \frac{1}{2}, \ell + 1; \gamma_\alpha\right)} > 0 \end{aligned} \quad (\text{C3})$$

for  $q > 0$ . We conclude that Eq. (C2) is not satisfied and that Eq. (23) has no solutions for  $q > 0$ , implying that there are no bound states of angular momenta  $\ell \geq \gamma_\alpha$ .

#### 2. Onset of bound states in finite size

##### a. Case $p = 0$

Although (41) has, in general, no closed form solution, we can obtain an approximate solution for the state  $p = 0$  of each angular momentum  $\ell$ , since the onset of that state will take place for small values of  $\lambda_\ell$  whenever  $R \gg \xi$ . We may thus solve

$$\Lambda_{\ell*} = \frac{\xi}{\alpha R} \quad (\text{C4})$$

to leading order in  $\lambda_\ell$ , with  $\Lambda_{\ell*} \equiv \Lambda_\ell(\lambda_{\ell*})$  the function given by Eq. (29)

The function  $\theta_\ell$  specified in Eq. (27) can be Taylor-expanded around  $\lambda_\ell \geq 0$  to leading order as

$$\theta_\ell = \begin{cases} \frac{\pi}{2} - \gamma_\alpha + \mathcal{O}(\gamma_\alpha^2) & , \ell = 0 \\ -a_\ell \lambda_\ell + \mathcal{O}(\lambda_\ell^3) & , \ell \geq 1 \end{cases},$$

with

$$a_\ell = \left(1 + \frac{1}{\ell}\right) \frac{M\left(\frac{1}{2}, \ell + 1; \ell\right)}{M\left(\frac{3}{2}, \ell + 2; \ell\right)},$$

by virtue of the derivative of the CHF satisfying [44]

$$M'(a, b; z) = \frac{a}{b} M(a + 1, b + 1; z).$$

Note that, for  $\ell \geq 1$ , we must first express  $\gamma_\alpha$  to leading order in  $\lambda_\ell$ , given by  $\gamma_\alpha = \ell + \lambda_\ell^2/(2\ell) + \mathcal{O}(\lambda_\ell^4)$ . In turn, Eq. (B5) gives  $\varphi_\ell = -\gamma_E \lambda_\ell + \mathcal{O}(\lambda_\ell^3)$  to leading order in  $\lambda_\ell$ .

We begin with the case  $\ell \geq 1$ . Eq. (C4) becomes, to leading order in  $\lambda_\ell$ ,

$$\frac{\sqrt{2}}{\ell} \exp\left(-\frac{\pi}{\lambda_{\ell*}}\right) e^{a_\ell - \gamma_E} = \frac{\xi}{\alpha R},$$

which can be rearranged to yield

$$\lambda_{\ell*} = \frac{\pi}{\log\left(\frac{R}{\xi r_{0,\ell}}\right)} \left(1 + \mathcal{O}(\lambda_{\ell*}^2)\right),$$

TABLE I. Results of the fits (C11) to the data from (C10) for values of  $c_{p,\ell}$  (top) and  $\ln(1/r_{p,\ell})$  (bottom).

| $p$        | 0                | 1                | 2                | 3                | 4                |
|------------|------------------|------------------|------------------|------------------|------------------|
| $\ell = 0$ | 0.7251<br>1.0826 | 0.2365<br>0.2642 | 0.1357<br>0.2493 | 0.0932<br>0.4039 | 0.0706<br>0.5555 |
| $\ell = 1$ | 0.3248<br>1.0191 | 0.1674<br>0.6487 | 0.1130<br>0.4144 | 0.0843<br>0.3376 | 0.0663<br>0.3721 |
| $\ell = 2$ | 0.3133<br>0.1441 | 0.1554<br>0.2474 | 0.1042<br>0.2653 | 0.0786<br>0.2562 | 0.0629<br>0.2713 |

with  $r_{p=0,\ell} = e^{\gamma_E - a_\ell} \sqrt{3\ell^2/5}$ . Squaring this result, Eq. (41) yields

$$\frac{g_{12}m_2}{g_{11}m_1} > \alpha^2 \ell^2 + \frac{c_{0,\ell}^{-2}}{\log\left(\frac{R}{\xi r_{0,\ell}}\right)^2}, \quad (\text{C5})$$

with  $c_{p=0,\ell} = \pi^{-1} \sqrt{6/5}$ . Higher-order terms in  $\log(R/r_{0,\ell})^{-1}$  can be obtained by expanding  $\theta_\ell$ ,  $\varphi_\ell$  and  $\gamma_\alpha$  to subleading order in  $\lambda_\ell$ , but these are found to be negligible.

For the case  $\ell = 0$ , we may take Eq. (C4) to leading order in  $\gamma_\alpha$  and rearrange it as

$$\gamma_{\alpha*} = \frac{3\pi}{2} \frac{1}{1 - \gamma_E - \log\left(\frac{\xi \gamma_{\alpha*}}{\sqrt{2}\alpha R}\right)}. \quad (\text{C6})$$

We note that for  $R \gg \xi$ , the RHS of (??) depends very weakly on  $\gamma_{\alpha*}$ ; indeed, numerical evidence indicates that the solution  $\gamma_{\alpha*} = \gamma_{\alpha*}(R)$ , for each  $R$ , is well approximated to zeroth order in  $R$  by  $\gamma_{\alpha*}(R) \approx \gamma_E$  over a range  $200 < R/\xi < 2000$ . Then, we may write  $\gamma_{\alpha*} = \gamma_E + \gamma_E \delta_*$ , with  $\delta_* = \gamma_{\alpha*}/\gamma_E - 1 \ll 1$  small, by hypothesis, so that we can take (C6) to leading order in  $\delta_*$  to yield

$$\gamma_{\alpha*} = \frac{\frac{3\pi}{2} - \gamma_E}{\log\left(\frac{R}{\xi r_{0,0}}\right)}, \quad (\text{C7})$$

with  $r_{0,0} = e^{\gamma_E} \sqrt{3\gamma_E^2/5}$ . Finally, squaring this result, Eq. (41) yields

$$\frac{g_{12}m_2}{g_{11}m_1} > \frac{c_{0,0}^{-2}}{\log\left(\frac{R}{\xi r_{0,0}}\right)^2}, \quad (\text{C8})$$

with  $c_{0,0} = (3\pi/2 - \gamma_E)^{-1} \sqrt{6/5}$ . These results suggest we can establish a law

$$\frac{g_{12}m_2}{g_{11}m_1} > \alpha^2 \ell^2 + \frac{c_{0,\ell}^{-2}}{\log\left(\frac{R}{\xi r_{0,\ell}}\right)^2}, \quad (\text{C9})$$

valid, at least, for  $p = 0$ .

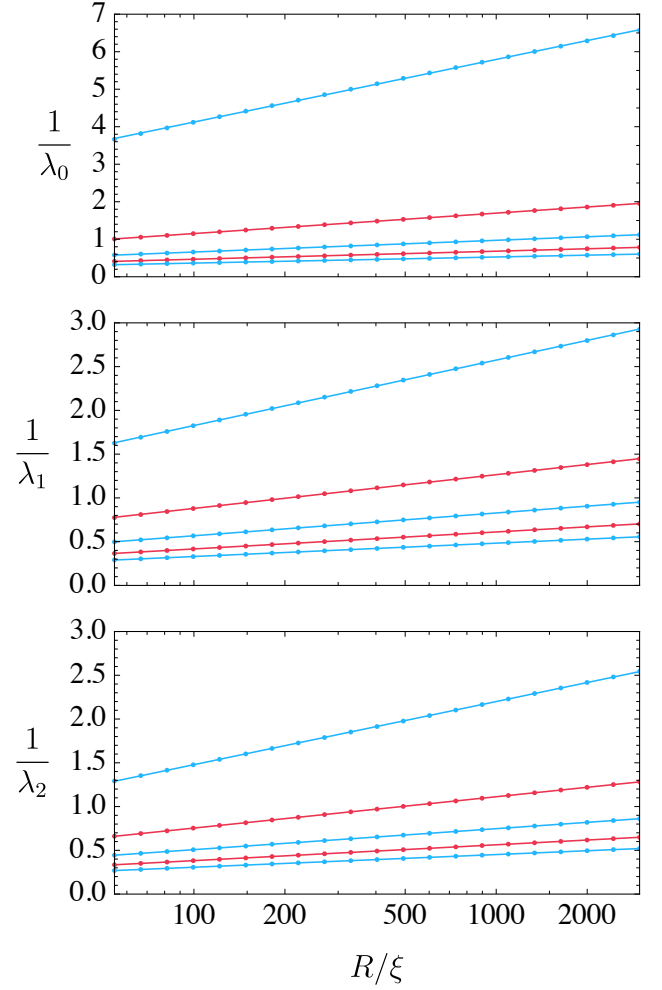


FIG. 7. (color online) Comparisons of the fits (C11) to the data from (C10) for  $\ell = 0$  (top),  $\ell = 1$  (middle) and  $\ell = 2$  (bottom), for  $p = 0, 1, 2, 3, 4$  in descending order on the plots for each  $\ell$ . The horizontal axis  $R/\xi$  is in logarithmic scale.

#### b. Case $p \geq 0$

In general, the foregoing considerations in the derivations of (C5) and (C8) no longer hold. However, we can show that condition (C9) is accurate as well for  $p \geq 1$ : we obtain numerical solutions of Eq. (C4) over a range  $50 < R/\xi < 3000$ , by employing a Newton method to the equation

$$\ln \Lambda_{\ell*} = -\ln \frac{\alpha R}{\xi}; \quad (\text{C10})$$

we then perform a linear fit of the expression on the RHS of (C9) to parameters  $c_{p,\ell}$  and  $r_{p,\ell}$  in a  $1/\lambda_\ell$  vs.  $\ln(R/\xi)$  plot, i.e.

$$\frac{1}{\lambda_\ell} = c_{p,\ell} \left( \ln \frac{R}{\xi} - \ln r_{p,\ell} \right). \quad (\text{C11})$$

Graphical comparisons are displayed in Fig. 7, while results of the fit are given in Table. I for a few bound

states. We thus conclude that Eq. (42) provides a condi-

tion for the onset of any bound state ( $p, \ell$ ).

- 
- [1] E. B. Gordon and A. F. Shestakov, *Low Temperature Physics* **26**, 1 (2000).
  - [2] J. T. Devreese, *Physics Today* **67**, 54 (2014).
  - [3] M. I. Dykman and E. I. Rashba, *Physics Today* **68**, 10 (2015).
  - [4] T. Vojta, *Annual Review of Condensed Matter Physics* **10**, 233 (2019).
  - [5] J. T. Devreese, “Polarons,” in *digital Encyclopedia of Applied Physics* (American Cancer Society, 2003).
  - [6] M. Drescher, M. Salmhofer, and T. Enss, *Phys. Rev. A* **99**, 023601 (2019).
  - [7] S. M. Yoshida, S. Endo, J. Levinsen, and M. M. Parish, *Phys. Rev. X* **8**, 011024 (2018).
  - [8] H. Fröhlich, H. Pelzer, and S. Zienau, *The London, Edinburgh, and Dublin Philosophical Magazine and Journal of Science* **41**, 221 (1950).
  - [9] G. Grimvall, *The Electron-Phonon Interaction in Metals (Selected Topics in Solid State Physics XVI)* (North-Holland Pub. Co. : sole distributors for the U.S.A. and Canada, Elsevier North-Holland, 1981).
  - [10] D. Stamatis, *Understanding ISO 9000 and Implementing the Basics to Quality (Quality and Reliability)* (CRC Press, 1995).
  - [11] A. G. Swartz, H. Inoue, T. A. Merz, Y. Hikita, S. Raghu, T. P. Devereaux, S. Johnston, and H. Y. Hwang, *Proceedings of the National Academy of Sciences* **115**, 1475 (2018), <https://www.pnas.org/content/115/7/1475.full.pdf>.
  - [12] J. Appel, *Phys. Rev.* **180**, 508 (1969).
  - [13] B. Gerlach and H. Löwen, *Rev. Mod. Phys.* **63**, 63 (1991).
  - [14] E. K. Kudinov, *Physics of the Solid State* **44**, 692 (2002).
  - [15] C. Grimaldi, *Phys. Rev. B* **77**, 024306 (2008).
  - [16] C. Grimaldi, *Phys. Rev. B* **81**, 075306 (2010).
  - [17] R. L. Frank and B. Schlein, *Letters in Mathematical Physics* **104**, 911 (2014).
  - [18] J. Tempere, W. Casteels, M. K. Oberthaler, S. Knoop, E. Timmermans, and J. T. Devreese, *Phys. Rev. B* **80**, 184504 (2009).
  - [19] J. Catani, G. Lamporesi, D. Naik, M. Gring, M. Inguscio, F. Minardi, A. Kantian, and T. Giamarchi, *Phys. Rev. A* **85**, 023623 (2012).
  - [20] R. Scelle, T. Rentrop, A. Trautmann, T. Schuster, and M. K. Oberthaler, *Phys. Rev. Lett.* **111**, 070401 (2013).
  - [21] N. B. Jørgensen, L. Wacker, K. T. Skalmstang, M. M. Parish, J. Levinsen, R. S. Christensen, G. M. Bruun, and J. J. Arlt, *Phys. Rev. Lett.* **117**, 055302 (2016).
  - [22] S. I. Mistakidis, G. C. Katsimiga, G. M. Koutentakis, T. Busch, and P. Schmelcher, *Phys. Rev. Lett.* **122**, 183001 (2019).
  - [23] L. A. Peña Ardila, N. B. Jørgensen, T. Pohl, S. Giorgini, G. M. Bruun, and J. J. Arlt, *Phys. Rev. A* **99**, 063607 (2019).
  - [24] A. A. Pelmenev, I. N. Krushinskaya, I. B. Bykhalo, and R. E. Boltnev, *Low Temperature Physics* **42**, 224 (2016).
  - [25] C. F. Barenghi, L. Skrbek, and K. R. Sreenivasan, *Proceedings of the National Academy of Sciences* **111**, 4647 (2014).
  - [26] J. M. Escartín, F. Ancilotto, M. Barranco, and M. Pi, *Phys. Rev. B* **99**, 140505 (2019).
  - [27] I. A. Pshenichnyuk, *New Journal of Physics*, **19**, 105007 (2017).
  - [28] J. R. Abo-Shaeer, C. Raman, J. M. Vogels, and W. Ketterle, *Science* **292**, 476 (2001).
  - [29] Y.-J. Lin, R. L. Compton, K. Jiménez-García, J. V. Porto, and I. B. Spielman, *Nature* **462**, 628 (2009).
  - [30] K. W. Madison, F. Chevy, W. Wohlleben, and J. Dalibard, *Physical Review Letters* **84**, 806 (2000).
  - [31] M. R. Matthews, B. P. Anderson, P. C. Haljan, D. S. Hall, C. E. Wieman, and E. A. Cornell, *Physical Review Letters* **83**, 2498 (1999).
  - [32] M. F. Andersen, C. Ryu, P. Cladé, V. Natarajan, A. Vaziri, K. Helmerson, and W. D. Phillips, *Phys. Rev. Lett.* **97**, 170406 (2006).
  - [33] V. Schweikhard, I. Coddington, P. Engels, V. P. Mogenendorff, and E. A. Cornell, *Physical Review Letters* **92** (2004), 10.1103/physrevlett.92.040404.
  - [34] A. A. Svidzinsky and A. L. Fetter, *Phys. Rev. Lett.* **84**, 5919 (2000).
  - [35] M. I. Shaukat, E. V. Castro, and H. Terças, *Physical Review A* **95**, 053618 (2017).
  - [36] M. I. Shaukat, E. V. Castro, and H. Terças, *Physical Review A* **98**, 022319 (2018).
  - [37] M. I. Shaukat, E. V. Castro, and H. Terças, *Physical Review A* **99**, 042326 (2019).
  - [38] L. Pitaevskii and S. Stringari, *Bose-Einstein Condensation (International Series of Monographs on Physics)* (Clarendon Press, 2003).
  - [39] C. J. Pethick and H. Smith, *Bose-Einstein Condensation in Dilute Gases*, 2nd ed. (Cambridge University Press, 2008).
  - [40] Y. Kawaguchi and T. Ohmi, *Phys. Rev. A* **70**, 043610 (2004).
  - [41] A. Cidrim, A. C. White, A. J. Allen, V. S. Bagnato, and C. F. Barenghi, *Phys. Rev. A* **96**, 023617 (2017).
  - [42] N. Manton and P. Sutcliffe, *Cambridge Monographs on Mathematical Physics* (Cambridge University Press, Cambridge, 2004).
  - [43] K. Konishi and G. . . Paffuti, *Quantum mechanics: a new introduction* (Oxford University Press, 2009).
  - [44] F. W. Olver, D. W. Lozier, R. F. Boisvert, and C. W. Clark, *NIST Handbook of Mathematical Functions*, 1st ed. (Cambridge University Press, New York, NY, USA, 2010).
  - [45] T. M. Dunster, *SIAM Journal on Mathematical Analysis*, *SIAM Journal on Mathematical Analysis* **21**, 995 (1990).
  - [46] E. Lundh, C. J. Pethick, and H. Smith, *Physical Review A* **58**, 4816 (1998).
  - [47] F. Schäfer, N. Mizukami, P. Yu, S. Koibuchi, A. Bouscal, and Y. Takahashi, *Physical Review A* **98**, 051602 (2018).
  - [48] N. Gross and L. Khaykovich, *Physical Review A* **77**, 023604 (2008).
  - [49] L. Salasnich, A. Parola, and L. Reatto, *Phys. Rev. A* **65**, 043614 (2002).
  - [50] P. Krüger, Z. Hadzibabic, and J. Dalibard, *Phys. Rev. Lett.* **99**, 040402 (2007).



- [51] L. E. Young-S., L. Salasnich, and S. K. Adhikari, *Phys. Rev. A* **82**, 053601 (2010).
- [52] W. Zhang, G.-D. Lin, and L.-M. Duan, *Phys. Rev. A* **78**, 043617 (2008).
- [53] A. L. Gaunt, T. F. Schmidutz, I. Gotlibovych, R. P. Smith, and Z. Hadzibabic, *Phys. Rev. Lett.* **110**, 200406 (2013).
- [54] I. Gotlibovych, T. F. Schmidutz, A. L. Gaunt, N. Navon, R. P. Smith, and Z. Hadzibabic, *Phys. Rev. A* **89**, 061604 (2014).
- [55] L. Chomaz, L. Corman, T. Bienaimé, R. Desbuquois, C. Weitenberg, S. Nascimbène, J. Beugnon, and J. Dalibard, *Nature Communications* **6**, 6162 (2015).
- [56] R. Desbuquois, T. Yefsah, L. Chomaz, C. Weitenberg, L. Corman, S. Nascimbène, and J. Dalibard, *Phys. Rev. Lett.* **113**, 020404 (2014).
- [57] A. M. Essin and D. J. Griffiths, *American Journal of Physics*, *American Journal of Physics* **74**, 109 (2006).
- [58] G. Catelani and E. A. Yuzbashyan, *Physical Review A* **81**, 033629 (2010).
- [59] A. H. Hansen, A. Y. Khramov, W. H. Dowd, A. O. Jamison, B. Plotkin-Swing, R. J. Roy, and S. Gupta, *Phys. Rev. A* **87**, 013615 (2013).
- [60] A. Khramov, A. Hansen, W. Dowd, R. J. Roy, C. Makrides, A. Petrov, S. Kotochigova, and S. Gupta, *Phys. Rev. Lett.* **112**, 033201 (2014).
- [61] M. A. Caracanhas, V. S. Bagnato, and R. G. Pereira, *Phys. Rev. Lett.* **111**, 115304 (2013).
- [62] L. U. Ancarani and G. Gasaneo, *Journal of Mathematical Physics*, *Journal of Mathematical Physics* **49**, 063508 (2008).
- [63] In the present work, we avoid the usual notation for the incomplete gamma function as to avoid any ambiguities with the parameter  $\gamma$ . ().
- [64] F. W. Olver, *Asymptotics and Special Functions*, 1st ed. (A K Peters/CRC, New York, NY, USA, 1997).
- [65] A. Jeffrey and D. Zwillinger, *Table of Integrals, Series, and Products* (Elsevier Science, 2007).
- [66] We disregard the condition  $\text{Re}\beta > 0$  by the convergence argument presented following Eq. (B20) and due to the fact that the integral in Eq. (B25) exists formally even for  $\text{Re}\beta = 0$ . ().
- [67] W. Magnus, F. Oberhettinger, and R. Soni, *Formulas and Theorems for the Special Functions of Mathematical Physics* (Springer Berlin Heidelberg, 2013).